General Model of Photon-Pair Detection with an Image Sensor

Hugo Defienne, Matthew Reichert, and Jason W. Fleischer

General model of photon-pair detection with an image sensor

Hugo Defienne,* Matthew Reichert, and Jason W. Fleischer

Department of Electrical Engineering, Princeton University, Princeton, NJ 08544, USA

(Dated: April 18, 2018)

We develop an analytic model that relates intensity correlation measurements performed by an image sensor to the properties of photon pairs illuminating it. Experiments using both an effective single-photon counting (SPC) camera, a linear electron-multiplying charge-coupled device (EMCCD) camera and a standard CCD camera confirm the model. The results open the field of quantum optical sensing using conventional detectors.

Because it may exhibit quantum features at room temperature, light is one of the most promising platforms to investigate quantum mechanics and its applications in quantum computing, communication, and imaging [1]. Pairs of photons represent the simplest system showing genuine quantum entanglement in all their degrees of freedom: spatial, spectral, and polarization [2–4]. Demonstrations range from fundamental tests of Bell's inequality with polarization entangled photons [5] to the development of new imaging techniques [6]. Spatial entanglement between photons is particularly attractive, since its natural high-dimensional structure [7, 8] holds promise for powerful information processing algorithms [9, 10] and secure cryptographic protocols [11, 12]. While generating photon pairs entangled over a large number of spatial positions is now commonly achieved using spontaneous parametric down-conversion (SPDC) [13], full characterization of entangled photon states in high-dimensional Hilbert spaces remains a challenging task. Indeed, the process requires intensity correlation measurements between all pairs of possible positions, and its efficiency strongly depends on the properties of the detection system.

Light intensity correlation is a type of optical measurement used in imaging techniques, such as scintigraphy [14] and ghost imaging [15], and in some characterization procedures, such as dynamic light scattering [16] and fluorescence correlation spectroscopy [17]. In quantum optics, intensity correlation measurements are used to measure coincidences between correlated photons. The detection apparatus generally involves single-photon sensitive devices connected to an electronic coincidence counting circuit. The number of measurements required scales with both the number of correlated photons and the number of optical modes. Typically, correlation measurements of spatially entangled photon pairs are performed with two avalanche photodiodes (APDs) that are raster-scanned over the different positions. Since pairs generated by a conventional SPDC source may be entangled over a very large number of spatial modes [18, 19], this raster scanning technique is prohibitively time consuming and cannot be used in practice.

Both electron multiplying (EM) [20–22] and intensified CCD [23] cameras have been used to perform high-dimensional measurements. A threshold applied on the measured images allows them to operate effectively as multi-pixel single-photon counters [24, 25]. Recent works have revealed some features of entanglement between pairs of photons generated by SPDC [20, 21], but these techniques have not retrieved the full characteristics the photon pairs, i.e., their full joint probability distribution. Moreover, the theoretical analyses associated with these works were carried out under approximations on the form of the correlation [26–28]. In particular, these works assumed a regime of detection in which the two photons never hit the same pixel of the camera, which is counterintuitive when measuring pairs that are strongly correlated in position.

In this work, we provide a general theoretical framework for intensity correlation measurements of two-photon states with any type of detection system, with no other approximations made on the source. We then compare our model to experiments performed with different detection systems: 1) an APD-like single-photon counter (SPC) camera, implemented using an EMCCD camera with thresholding [19], 2) a linear EMCCD camera with no threshold and 3) a standard CCD camera. Surprisingly, we show that the joint probability distribution of entangled photon pairs can be measured using standard CCD cameras without thresholding, which provides one of the simplest techniques to characterize high-dimensional spatial entanglement of photon pairs.

Figure 1 shows the general detection scheme considered in our model. It is studied with respect to two assumptions :

(i) Pixels of the image sensor operate independently

(ii) The input state is a pure two-photon state

In the input, denoted $|\phi\rangle$, both photons have the same polarization and frequency spectrum. Its associated two-photon wavefunction depends only on the spatial properties of the pairs [29] and can be expressed as

$$|\phi\rangle = \sum_{i,j\in[\![1,N]\!]} \phi_{ij}|i,j\rangle \tag{1}$$

where $|i,j\rangle$ is a non-symmetric state defining a configuration in which the first photon of a pair is located at
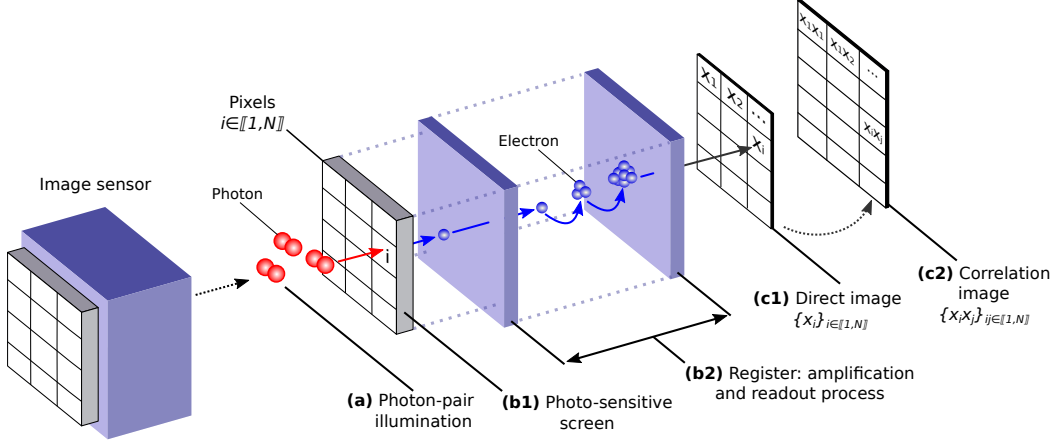
---

* defienne@princeton.edu

Figure 1. **Schematic of the detection architecture.** (a) A pure photon-pair state illuminates (b) the image sensor that (c) returns two types of images at the output. Distribution of photon pairs at the input is determined by the joint probability distribution Γ_{ij}, where i and j are two pixels of the sensor. During the exposure time photons arrive at (b1) the photo-sensitive screen and are transformed into photoelectrons with probability η. Photoelectrons in each pixel are (b2) amplified and converted into measurable signals during the readout process (c1) A direct image $\{x_i^{(l)}\}_{i\in[\![1,N]\!]}$ and (c2) a correlation image $\{x_i^{(l)}x_j^{(l)}\}_{i,j\in[\![1,N]\!]}$ are returned by the detector after each acquisition.

pixel i and the second at pixel j, and ϕ_{ij} is the spatially dependent two-photon wavefunction discretized over the pixels of the sensor. The joint-probability distribution $\Gamma_{ij} = |\phi_{ij}|^2$ represents the probability of the first photon of the pair arriving at pixel i and the second at pixel j.

Each photon falling on the camera has a probability η to be transformed into a photoelectron. In addition, electrons can also be generated from thermal fluctuations (dark noise). As shown in Figure 1, input electrons go through a potential amplification and readout process that converts them into detectable signals. The exact operation performed depends only on the internal characteristics of the image sensor, including the specific sensor technology and its noise properties. This process is then fully characterized by a set of conditional probability functions $\{P(x_i|k_i)\}_{i\in[\![1,N]\!]}$, in which $k_i \in \mathbb{N}$ is the number of electrons present at pixel i after the screen and x_i the corresponding output value returned by the sensor. Henceforth, we refer to $\{P(x_i|k_i)\}_{i\in[\![1,N]\!]}$ as the detector response function.

Two types of images are returned at the output at the lth acquisition: a direct image, denoted $\{x_i^{(l)}\}_{i\in[\![1,N]\!]}$, composed of output values returned at each pixel, and a correlation image, denoted $\{x_i^{(l)}x_j^{(l)}\}_{i,j\in[\![1,N]\!]}$, computed by the tensor product of each direct image with itself. When a large number of images M is recorded, averaging over all of them enables estimation of the mean values:

$$\langle x_i \rangle = \lim_{M\to\infty} \frac{1}{M} \sum_{l=0}^{M} x_i^{(l)} \tag{2}$$

$$\langle x_i x_j \rangle = \lim_{M\to\infty} \frac{1}{M} \sum_{l=0}^{M} x_i^{(l)} x_j^{(l)} \tag{3}$$

Assuming stationary illumination, $\langle x_i \rangle$ and $\langle x_i x_j \rangle$ can be

written in term of their corresponding probability distributions:

$$\langle x_i \rangle = \sum_{x_i=0}^{+\infty} x_i\, P(x_i) \tag{4}$$

$$\langle x_i x_j \rangle = \sum_{x_i=0}^{+\infty} \sum_{x_j=0}^{+\infty} x_i x_j\, P(x_i, x_j) \tag{5}$$

where $P(x_i)$ represents the probability for the sensor to return value x_i at pixel i and $P(x_i, x_j)$ is the joint probability to return values x_i at pixel i and x_j at pixel j, during the acquisition of each frame. Using Bayes' theorem, $\langle x_i \rangle$ can be expressed as:

$$\langle x_i \rangle = \sum_{m=0}^{+\infty} P(m) \sum_{k_i=0}^{2m} I_{k_i} P(k_i|m) \tag{6}$$

where $P(m)$ is the probability for $m \in \mathbb{N}$ pairs to fall on the screen during the exposure time and $P(k_i|m)$ is the conditional probability of generating k_i photoelectrons at pixel i given m pairs. I_{k_i} is the mean of the detector response function at pixel i, defined as:

$$I_{k_i} = \sum_{x_i=0}^{+\infty} x_i\, P(x_i|k_i) \tag{7}$$

$P(k_i|m)$ can then be written in terms of the marginal probability $\Gamma_i = \sum_i \Gamma_{ij}$ and the probability of measuring both photons of a pair at the same pixel Γ_{ii}. The complete calculation is detailed in Appendix A, and leads to the following general expression for $\langle x_i \rangle$:

$$\langle x_i \rangle = \sum_{m=0}^{+\infty} P(m) \sum_{k_i=0}^{2m} I_{k_i} \sum_{q=0}^{\lfloor k_i/2 \rfloor} \left(\eta^2 \Gamma_{ii}\right)^q \left(2\eta\,\Gamma_i - 2\eta^2\Gamma_{ii}\right)^{k_i-2q} \left(1 - 2\eta\,\Gamma_i + \eta^2\Gamma_{ii}\right)^{m-k_i+q} \binom{k_i - q}{q} \binom{m}{k_i - q} \quad (8)$$

where $\binom{n}{k} = \frac{n!}{k!(n-k)!} H(n-k)$, H is the Heaviside (unit step) function. Using a similar approach, the correlation image $\langle x_i x_j \rangle$ for the system to return a value x_i at pixel i and x_j at pixel $j \neq i$ is written as:

$$\langle x_i x_j \rangle = \sum_{m=0}^{+\infty} P(m) \sum_{k_i=0}^{2m} \sum_{k_j=0}^{2m} I_{k_i} I_{k_j} P(k_i, k_j | m) \quad (9)$$

where $P(k_i, k_j | m)$ is the conditional probability of generating k_i and k_j photoelectrons at pixels i and $j \neq i$, respectively, given m photon pairs in each frame. Assuming that η is uniform over the screen, the correlation coefficient $\langle x_i x_j \rangle$ can be related to the Γ_{ij}. The full calculation, given in appendix B, gives:

$$\langle x_i x_j \rangle = \sum_{m=0}^{+\infty} P(m) \sum_{k_i=0}^{2m} \sum_{k_j=0}^{2m} I_{k_i} I_{k_j} \sum_{q=0}^{\lfloor (k_i+k_j)/2 \rfloor} \sum_{l=0}^{q} \sum_{p=0}^{q-l} (1 - 2\eta\Gamma_i - 2\eta\Gamma_j + \eta^2\Gamma_{ii} + \eta^2\Gamma_{jj} + 2\eta^2\Gamma_{ij})^{m-(k_i+k_j-q)}$$
$$\left(\eta^2\Gamma_{jj}\right)^p \left(2\eta^2\Gamma_{ij}\right)^l \left(\eta^2\Gamma_{ii}\right)^{q-l-p} (2\eta\Gamma_i - 2\eta^2\Gamma_{ii} - 2\eta^2\Gamma_{ij})^{k_i+l-2(q-p)} (2\eta\Gamma_j - 2\eta^2\Gamma_{jj} - 2\eta^2\Gamma_{ij})^{k_j-2p-l}$$
$$\binom{k_j - l - p}{p} \binom{k_i - q + p}{q - l - p} \binom{k_i + k_j - q - l}{k_i - q + p} \binom{k_i + k_j - q}{l} \binom{m}{k_i + k_j - q} \quad (10)$$

Equations 8 and 10 show that knowing the characteristics of the image sensor, namely its quantum efficiency and response function, as well as the number distribution of incident pairs $P(m)$, relates the direct images, $\langle x_i \rangle$ and $\langle x_j \rangle$, and the correlation image, $\langle x_i x_j \rangle$, to the joint probability distribution of the pairs Γ_{ij}. Note that these results hold only for $i \neq j$; the case $i = j$ is more subtle and is treated separately in appendix H.

This set of equations provides a general link between measurements performed by any detector and the joint probability distribution of photon pairs illuminating it. We demonstrate the validity of our model by applying it to the cases of an SPC camera, mimicked using a thresholded EMCCD camera [19], an EMCCD camera operated without threshold, and a standard CCD camera.

SPC cameras generally consist of an array of single-photon avalanche diodes (SPADs) or APDs with all electronics incorporated into each pixel. Photon-to-electron conversion is performed at a given quantum efficiency η, and the detector ideally returns a non-null current (value 1) at the output if at least one electron was present at the input of the amplifier and no current if not (value 0). As shown in appendix C, assuming a Poissonian distribution [30] for $P(m)$ in this model simplifies Equations 8 and 10, allowing expression of Γ_{ij} in terms of $\langle c_i \rangle$ and $\langle c_i c_j \rangle$:

$$\Gamma_{ij} = \frac{1}{2\eta^2 \bar{m}} \ln \left[1 + \frac{\langle c_i c_j \rangle - \langle c_i \rangle \langle c_j \rangle}{(1 - \langle c_i \rangle)(1 - \langle c_j \rangle)} \right] \quad (11)$$

where the general output variable x has been replaced by a binary variable c (counts) that takes only two possible values $c \in \{0, 1\}$. The mean photon-pair rate $\bar{m}$, which can be controlled by adjusting the exposure time of the sensor or the power of the pump laser, and the quantum efficiency η act only as scaling factors.

Experimental results are shown in Figure 2. Pairs are generated by type-I SPDC in a β-barium borate (BBO) crystal pumped by a continuous-wave (CW) laser centered at 403 nm, and near-degenerate down-conversion is selected via spectral filters at 806 ± 1.5 nm. The far field of the output of the BBO crystal is projected onto the screen of an EMCCD camera. As detailed in [19], applying a threshold on each acquired image effectively enables the EMCCD to operate as an SPC camera with quantum efficiency $\eta_{eff} \approx 0.44$ and a noise probability $p_{10} \approx 0.015$ (appendix D.c). To facilitate the analysis, the 4-dimensional space of pair positions is reduced to 2 dimensions by fixing the Y-coordinates $Y_1 = 33$ and $Y_2 = 45$ (arbitrarily) and measuring only $\langle c_i \rangle$ and $\langle c_i c_j \rangle$ along two X-axis pixels of the camera, denoted $\{X_1\}$ and $\{X_2\}$ (Figure 2.b). Figure 2.c shows the measured joint probability distribution $\Gamma_{X_1 X_2}$ together with the marginals Γ_{X_1} and Γ_{X_2} (taken after background subtraction and normalization, appendix G). The intense anti-diagonal reveals an anti-correlated behavior of the pairs, as expected when measuring photons in the far field of the crystal. As shown in Figure 2.d, the measured joint probability distribution is well fit by a double-Gaussian model [31] $\Gamma_{X_1 X_2}^{th}$ of parameters $\sigma_- = 926.1\,\mu m$ and $\sigma_+ = 12.1\,\mu m$ (appendix F). Selected profiles $\Gamma_{X_1 | X_2 = 65}$ and $\Gamma_{X_1 | X_2 = 65}^{th}$, highlighted in Figure 2.e, show a good match between the experiment and the double-Gaussian

fit, confirming the validity of our model.

It is commonly thought that photon counting is necessary to compute the joint probability distribution of pairs of photons. We now demonstrate the surprising result that simple operation of a camera without thresholding also enables measurement of Γ_{ij}. In this case, the readout process becomes more complex, but an analytic form of $P(x|k)$ can be calculated quantitatively if the sources of noise are known, e.g. those provided in [26]. For EM-CCD cameras, the mean of the detector response function I_k depends linearly on the number of electrons k at the input, $I_k = A\,k + x_0$, where the amplification parameter A depends on the mean gain and analog-to-digital conversion and x_0 is a constant background (Appendix D). As shown in Appendix E, this response allows expression

of Γ_{ij} as

$$\Gamma_{ij} = \frac{1}{2A^2\bar{m}\eta^2}\left[\langle x_i x_j\rangle - \langle x_i\rangle\langle x_j\rangle\right] \qquad (12)$$

where the parameters A, η and $\bar{m}$ contribute only a scaling factor, which may be determined by normalization.

The physical interpretation of Equation 12 can be seen by expanding the expression $R_{ij} \equiv \langle x_i x_j\rangle - \langle x_i\rangle\langle x_j\rangle$ over a finite number of images $M \gg 1$ using Equations 2 and 3:

$$R_{ij} \approx \frac{1}{M}\sum_{l=0}^{M} x_i^{(l)} x_j^{(l)} - \frac{1}{M^2}\sum_{l,l',l\neq l'}^{M} x_i^{(l)} x_j^{(l')} \qquad (13)$$

The first term is the average tensor product of each frame with itself. Intensity correlations in this term originate from detections of both real coincidences (two photons from the same entangled pair) and accidental coincidences (two photons from two different entangled pairs). Since there is zero probability for two photons from the same entangled pair to be detected in two different images, intensity correlations in the second term originate only from photons from different entangled pairs (accidental coincidence). A subtraction between these two
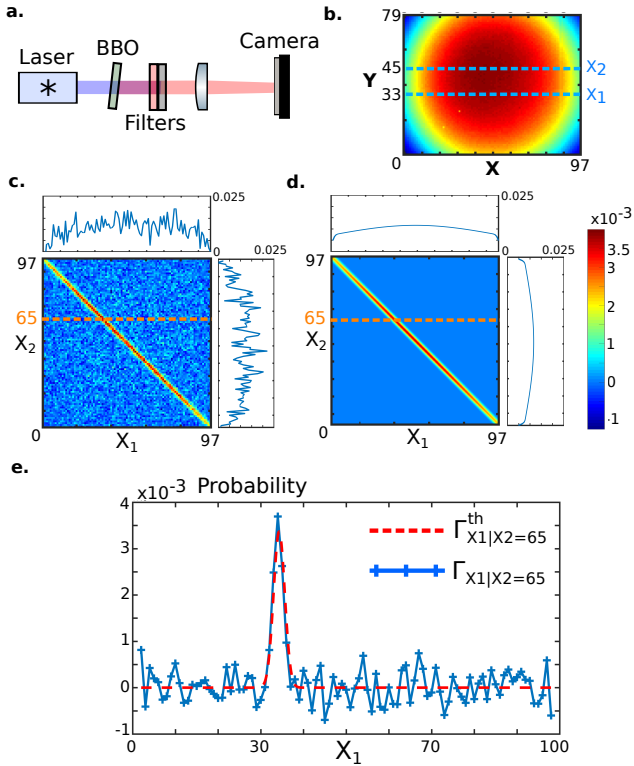

Figure 2. **Measurement of the joint probability distribution of photon pairs with an SPC camera.** (a) photon pairs generated by type I SPDC are Fourier-imaged onto the screen of an EMCCD camera operating at maximum gain $G = 1000$ and with a temperature maintained at $-60°$C. A threshold applied to every image acquired at the output enables this camera to operate as an SPC camera (Appendix D). (b) Averaged direct image, proportional to the marginal distribution Γ_i. (c) 2D slices of measured joint probability distribution $\Gamma_{X_1 X_2}$ at $Y_1 = 33$ and $Y_2 = 45$ [as indicated by dashed lines in (b)], and its marginals Γ_{X_1} and Γ_{X_2}. (d) Double-Gaussian model fit $\Gamma^{th}_{X_1 X_2}$ of the reconstructed joint probability distribution (Appendix F). (e) Profiles $\Gamma_{X_1|X_2=65}$ and $\Gamma^{th}_{X_1|X_2=65}$ showing the good accordance between the experiment and the double-Gaussian fit.
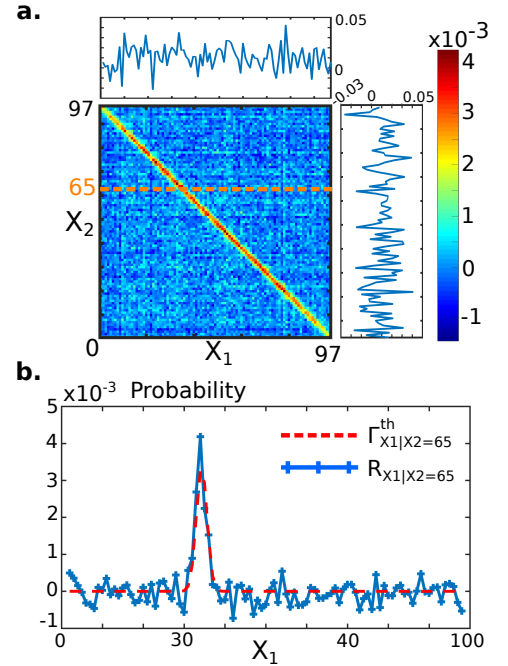

Figure 3. **Measurement of the joint probability distribution of photon pairs with a non-thresholded EM-CCD camera.** (a) $R_{X_1 X_2} = \langle x_{X_1} x_{X_2}\rangle - \langle x_{X_1}\rangle\langle x_{X_2}\rangle$ measured by performing an experiment in the same conditions as in Figure 2.a but without thresholding. After normalization and background subtraction, $R_{X_1 X_2}$ shows very good agreement with the theoretical model $\Gamma^{th}_{X_1 X_2}$ calculated for Figure 2.b. (b) Selected profiles $R_{X_1|X_2=65}$ (blue) and $\Gamma^{th}_{X_1|X_2=65}$ (red) confirm the good agreement. A total of 10^7 images were acquired with EM gain set to $G = 1000$, an exposure time of $2\,\text{ms}$ and a temperature maintained at $-60°$C.
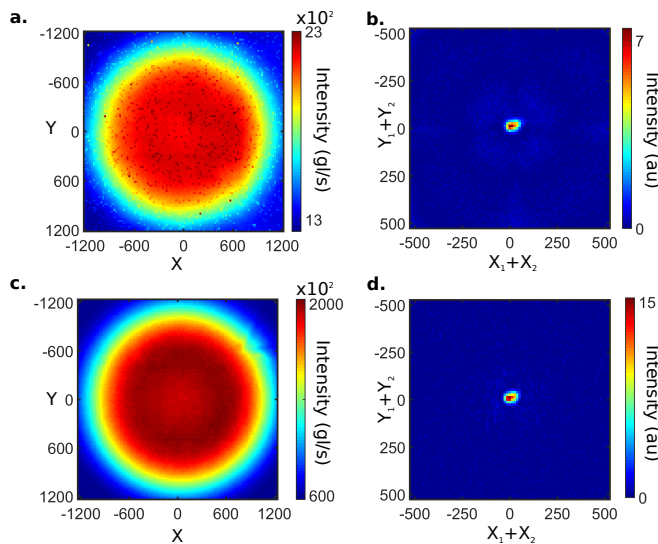
Figure 4. **Entanglement characterization with a standard CCD camera.** Averaged intensity image (a) and sum-coordinate projection of Γ (b) using a standard CCD camera. The peaks of intensity correlation at the center of the sum coordinate projections are clear signatures of strong anti-correlations between photons imposed by momentum conservation in the pair generation process. As a comparison, averaged intensity image (c) and sum-coordinate projection (d) measured using the EMCCD camera operating with a gain of $G = 1000$. A total 83160 images were acquired in both cases. The temperature is not maintained with the standard camera (room : $\sim 20^\circ$C) but is maintained with the EMCCD (-60°). (gl/s: grey level per second).

terms leaves only genuine coincidences, which is proportional to the joint probability distribution Γ_{ij}.

Experimental confirmation of Equation 12 using different detection schemes is shown in Figure 3 and 4. Figure 3.a shows the quantity $R_{X_1 X_2}$ measured by performing an experiment in the same conditions as that for Figure 2.a but without thresholding the output images. These results compare favorably with those of Figure 2.b. Profiles $R_{X_1|X_2=65}$ (blue) and $\Gamma^{th}_{X_1|X_2=65}$ (red) shown in Figure 3.c highlight the very good agreement between the double-Gaussian fit and the measurement without threshold.

Figure 4 shows a similar experiment performed using a standard CCD camera (Appendix I). To compensate for the lack of amplification, the exposure time is raised to 0.5s. Figure 4.b shows a projection of reconstructed Γ on the sum coordinates $\{X_1 + X_2, Y_1 + Y_2\}$. The strong peak of intensity correlation at its center is a clear signature of entanglement between photons due to momentum conservation in the pair generation process [20, 21]. The same experiment performed with the high gain EMCCD camera confirms this observation (Figure 4.d).

These results show that measuring quantum correlation between pairs of photons is not a task exclusive to single-photon sensitive devices such as SPC cameras, SPADs, or APD arrays but can be achieved using any type of image sensor. Using a megapixel image sensor as a highly parallel intensity correlator offers much promise for measuring high-dimensional entangled states, necessary for quantum computing, communication, and imaging. Moreover, the model can be extended readily to states containing more than two entangled photons, in order to study higher degrees or new forms of entanglement.

[1] I. A. Walmsley, Science **348**, 525 (2015).
[2] J. Brendel, N. Gisin, W. Tittel, and H. Zbinden, Phys. Rev. Lett. **82**, 2594 (1999).
[3] P. G. Kwiat, K. Mattle, H. Weinfurter, A. Zeilinger, A. V. Sergienko, and Y. Shih, Phys. Rev. Lett. **75**, 4337 (1995).
[4] J. C. Howell, R. S. Bennink, S. J. Bentley, and R. W. Boyd, Phys. Rev. Lett. **92**, 210403 (2004).
[5] A. Aspect, J. Dalibard, and G. Roger, Phys. Rev. Lett. **49**, 1804 (1982).
[6] G. Brida, M. Genovese, and I. R. Berchera, Nat Photon **4**, 227 (2010).
[7] R. Fickler, R. Lapkiewicz, W. N. Plick, M. Krenn, C. Schaeff, S. Ramelow, and A. Zeilinger, Science **338**, 640 (2012).
[8] M. Krenn, M. Huber, R. Fickler, R. Lapkiewicz, S. Ramelow, and A. Zeilinger, Proceedings of the National Academy of Sciences **111**, 6243 (2014).
[9] D. S. Tasca, R. M. Gomes, F. Toscano, P. H. Souto Ribeiro, and S. P. Walborn, Phys. Rev. A **83**, 052325 (2011).
[10] N. K. Langford, R. B. Dalton, M. D. Harvey, J. L. OBrien, G. J. Pryde, A. Gilchrist, S. D. Bartlett, and A. G. White, Physical review letters **93**, 053601 (2004).
[11] S. P. Walborn, D. S. Lemelle, D. S. Tasca, and P. H. Souto Ribeiro, Phys. Rev. A **77**, 062323 (2008).
[12] M. Mirhosseini, O. S. Magaa-Loaiza, M. N. OSullivan, B. Rodenburg, M. Malik, M. P. J. Lavery, M. J. Padgett, D. J. Gauthier, and R. W. Boyd, New J. Phys. **17**, 033033 (2015).
[13] A. A. Malygin, A. N. Penin, and A. V. Sergienko, in *Sov. Phys. Dokl*, Vol. 30 (1985) pp. 227–229.
[14] G. A. Digenis and E. Sandefer, Critical reviews in therapeutic drug carrier systems **7**, 309 (1991).
[15] T. B. Pittman, Y. H. Shih, D. V. Strekalov, and A. V. Sergienko, Phys. Rev. A **52**, R3429 (1995).
[16] B. J. Berne and R. Pecora, *Dynamic Light Scattering: With Applications to Chemistry, Biology, and Physics* (Courier Corporation, 2013).
[17] D. Magde, E. Elson, and W. W. Webb, Phys. Rev. Lett. **29**, 705 (1972).
[18] M. Reichert, X. Sun, and J. W. Fleischer, Physical Review A **95**, 063836 (2017).
[19] M. Reichert, H. Defienne, and J. W. Fleischer, arXiv:1710.01781 [physics, physics:quant-ph] (2017), arXiv: 1710.01781.
[20] P.-A. Moreau, J. Mougin-Sisini, F. Devaux, and

E. Lantz, Phys. Rev. A **86**, 010101 (2012).

[21] M. P. Edgar, D. S. Tasca, F. Izdebski, R. E. Warburton, J. Leach, M. Agnew, G. S. Buller, R. W. Boyd, and M. J. Padgett, Nature communications **3**, 984 (2012).

[22] E. Bolduc, D. Faccio, and J. Leach, J. Opt. **19**, 054006 (2017).

[23] M. Hamar, J. Peina, O. Haderka, and V. Michlek, Phys. Rev. A **81**, 043827 (2010).

[24] A. G. Basden, C. A. Haniff, and C. D. Mackay, Monthly Notices of the Royal Astronomical Society **345**, 985 (2003).

[25] A. Avella, I. Ruo-Berchera, I. P. Degiovanni, G. Brida, and M. Genovese, Opt. Lett., OL **41**, 1841 (2016).

[26] E. Lantz, J.-L. Blanchet, L. Furfaro, and F. Devaux, Monthly Notices of the Royal Astronomical Society **386**, 2262 (2008).

[27] D. S. Tasca, M. P. Edgar, F. Izdebski, G. S. Buller, and M. J. Padgett, Phys. Rev. A **88**, 013816 (2013).

[28] E. Lantz, P.-A. Moreau, and F. Devaux, Phys. Rev. A **90**, 063811 (2014).

[29] B. J. Smith and M. G. Raymer, New J. Phys. **9**, 414 (2007).

[30] T. S. Larchuk, M. C. Teich, and B. E. A. Saleh, Annals of the New York Academy of Sciences **755**, 680 (1995).

[31] M. V. Fedorov, Y. M. Mikhailova, and P. A. Volkov, J. Phys. B: At. Mol. Opt. Phys. **42**, 175503 (2009).